

Simulation of satellite channel radiances in the Met Office Unified Model

By M. A. RINGER*, J. M. EDWARDS and A. SLINGO

Met Office, Hadley Centre for Climate Prediction and Research, UK

(Received 13 February 2002; revised 6 September 2002)

SUMMARY

A system is described which allows satellite channel radiances to be simulated within both the numerical weather prediction and climate versions of the Met Office Unified Model. It is based on a spherical harmonics version of the radiation code that calculates radiative fluxes and heating rates in the climate model and it uses the same pre-processing software and molecular absorption database. In the results shown here, fractional cloud cover is represented by decomposition into separate columns. The methodology is described and results of off-line tests of the code against high spectral resolution calculations are presented. Examples of infrared window and water vapour channel brightness temperatures simulated using the global forecast model are then compared with Meteosat 7 imagery. The utility of radiance simulations for model validation studies is illustrated by these comparisons, and other applications are also discussed.

KEYWORDS: Model validation Radiative-transfer models Satellite radiances

1. INTRODUCTION

Satellite data provide important information for assessing the performance of climate models and for studying climate variability and trends. For these applications, the calibrated radiances are usually processed to produce high-level products, such as cloud amounts, radiative fluxes, precipitation rates and so on. Such products are very convenient for evaluating models, because the corresponding fields are produced routinely during model simulations, so that relatively little additional processing of the model output is required.

In contrast, in numerical weather prediction (NWP) it is now standard practice to use the radiances themselves and to assimilate them directly into a weather-forecast model by adjusting the model fields to minimize the difference between the observed radiances and those simulated by the model. This requires an accurate forward model to provide the simulated radiances, as well as knowledge of the error characteristics both of the model and of the data, so as to optimize the assimilation by variational methods (e.g. English *et al.* 2000). The advantage of using radiances as opposed to high-level products in NWP is that it preserves the information content of the data with the minimum of processing and enables a wide variety of data types to be assimilated, provided that there is a forward model available for each type.

There is increasing evidence that climate applications can also benefit from the use of radiances as opposed to high-level products. A number of studies (e.g. Soden and Bretherton 1994; Soden and Fu 1995; Salathé and Chesters 1995; Salathé *et al.* 1995) have focused on the representation of upper tropospheric moisture in models using simulations of radiance measurements in the 6.3 μm water vapour absorption band. In these studies model temperature and humidity profiles were used as input to a radiative-transfer model to calculate clear-sky radiances which were then compared with cloud-cleared radiance observations. Morcrette (1991) compared model-simulated brightness temperatures with those from Meteosat and demonstrated the potential of what he termed the ‘model-to-satellite approach’ for evaluating model-generated cloudiness.

* Corresponding author: Met Office, Hadley Centre for Climate Prediction and Research, London Road, Bracknell, Berkshire RG12 2SY, UK. e-mail: mark.ringer@metoffice.com

© Crown copyright, 2003.

This approach was pursued in further studies using Meteosat data by Duvel *et al.* (1996) and Roca *et al.* (1997), while Yu *et al.* (1997) presented comparisons of model-simulated brightness temperatures with GOES* measurements. More recently, Chevallier and Kelly (2002) have compared Meteosat infrared window imagery with simulations using the current version of the European Centre for Medium-Range Weather Forecasts model and a modified version of the fast code RTTOV† (Eyre 1991).

Data from geostationary satellites are particularly well suited to such applications, since they contain high-frequency information that may be exploited to reveal details of physical processes and interactions, both in the models and in the real world (e.g. Yang and Slingo 2001; Janowiak *et al.* 2001). The availability of long time series of quality controlled data from polar orbiting satellites provides opportunities for evaluating models on longer time-scales (e.g. Bates *et al.* 1996; Geer *et al.* 1999), although it may be important to take account of the infrequent sampling from satellites in low earth orbits (Engelen *et al.* 2000). For the detection and attribution of climate trends, it is important that the minimal of processing is applied to the satellite data and that spectrally resolved radiances are available (Goody *et al.* 1998).

The radiation scheme used to calculate fluxes and heating rates in the climate version of the Met Office Unified Model (Pope *et al.* 2000) is a two-stream code described by Edwards and Slingo (1996). A version of the scheme has recently been implemented in the NWP model. We have developed a radiance version that includes clouds and is based on the same molecular line database as the flux code. The trade-off between accuracy and speed can be chosen according to the particular application. Simulations of the radiances observed by a satellite instrument take into account the instrumental spectral response and the viewing geometry. The code is run within the model as an integration proceeds and is independent of the calculation of fluxes and heating rates, allowing the sampling to be adjustable. A full treatment of scattering is included and the code is consistent with the flux version (which calculates the heating rates used to advance the model) in its treatment of clouds, aerosols and gaseous absorption. This provides a sound basis for interpreting the differences between observed and simulated radiances in terms of the model variables. The code has primarily been developed for diagnostic purposes and, while it may not be fast enough for all possible applications (e.g. data assimilation), it does provide a standard against which simpler methods developed for particular purposes could be compared. The flexibility of the code is illustrated by the fact that it has also been used to simulate the radiances observed at high spectral resolution by spectrometers on research aircraft. Results from that work will be reported elsewhere.

In the following section, the methodology used to calculate radiances is described, including a brief description of the radiance code and of the technique used to combine the molecular absorption data with the instrumental spectral response. Section 3 describes the application of the code to the thermal infrared window and water vapour channels on the Meteosat 7 operational geostationary satellite and presents the results of tests against high spectral resolution calculations. Section 4 presents comparisons between simulations from NWP analyses and Meteosat data, illustrating the potential for evaluating physical processes in the model. The final section summarizes the work and discusses some of the planned future applications.

* Geostationary Operational Environmental Satellite.

† Radiative Transfer for TIROS (Television Infrared Observation Satellite) Operational Vertical Sounder.

2. METHODOLOGY

The total radiance at the top of the atmosphere measured by a satellite instrument over a spectral interval, $\Delta\nu$, is

$$I(p=0, \mu) = \frac{\int_{\Delta\nu} \phi(\nu) I_\nu(p=0, \mu) d\nu}{\int_{\Delta\nu} \phi(\nu) d\nu} \quad (1)$$

where I_ν is the monochromatic radiance, p is the pressure, μ is the cosine of the viewing angle and $\phi(\nu)$ is the instrument spectral response (or 'filter') function. In order to calculate this quantity in the Unified Model we need a general facility to calculate radiances combined with a method that accounts for the instrument response.

(a) *The radiation code*

A detailed description of the original version of the radiation code is given by Edwards and Slingo (1996). With regard to the present work, one of the most important design features of the code is that the spectral resolution is flexible, allowing it to be used across a wide variety of applications: providing reference calculations, simulating aircraft measurements and for use in forecast and climate modelling. This flexibility is achieved by reading in all the spectrally dependent information (the number of bands, the band limits, the absorbing species, the spectral properties of atmospheric constituents, etc.) at run time from a 'spectral file' created by a pre-processor. Once the required spectral files have been created, they may be stored for future use, so there is no need to re-run the pre-processor each time the radiation code is run. In order to simulate satellite channel radiances, we therefore need to create spectral files appropriate to the channel(s) under consideration.

(b) *Calculation of radiances*

A major consideration in the design of the two-stream code of Edwards and Slingo (1996) was the requirement of generality, which opens up a wide range of applications and facilitates the development of parametrizations for large-scale models: it is useful to aim for a similar level of generality in the simulation of radiances. Much of the infrastructure of the original code is applicable to the calculation of radiances, the key issue being the selection of an algorithm for the calculation of monochromatic radiances. Of the various methods available, we have chosen that of spherical harmonics as it provides a unified framework for the calculation of radiances and fluxes, and potentially photolysis rates. The algorithm is based on the method presented by Benassi *et al.* (1984), extended to multiple atmospheric layers. Assuming a plane-parallel atmosphere, the radiance, I , in a direction, \mathbf{n} , at an optical depth, τ , can be written as

$$I(\tau, \mathbf{n}) = \sum_{l=0}^{\infty} \sum_{m=-l}^l I_{lm}(\tau) Y_l^m(\mathbf{n}) \quad (2)$$

where the Y_l^m are the spherical harmonics, which obey the orthogonality relations,

$$\int_{\Omega} Y_l^m(\mathbf{n}) Y_{l'}^{m'}(\mathbf{n}) d\omega_{\mathbf{n}} = \delta_{ll'} \delta_{mm'} \quad (3)$$

where Ω represents integration over the sphere and $d\omega_{\mathbf{n}}$ is an element of solid angle about the direction \mathbf{n} . After imposing an order of truncation, L , the equation of transfer can be reduced to a set of ordinary differential equations for the I_{lm} in τ . This suffices

for the calculation of fluxes, but, because the series (2) may converge slowly along an individual ray, radiances are calculated by direct integration along that ray, using the spherical harmonic solution to define the scattered radiation field (Benassi *et al.* 1984). (In this formulation it is trivial to incorporate a higher order of truncation of the phase function in the calculation of singly scattered radiation at solar wavelengths, allowing us easily to employ the method of Nakajima and Tanaka (1988), which they designate solely by the abbreviation TMS.) For use in a large-scale model, the code is written to operate simultaneously on a vector of points. In the present study, fractional cloud cover is represented by decomposition into a number of separate columns, within each of which the cloud amount is either zero or unity in each layer, taking into account the overlap assumption. The number of columns used at each point depends on the cloud geometry and the specified overlap assumption. This is also an option in the original flux version, so that direct comparisons between flux and radiance calculations are possible. Simulations of the radiances observed by particular satellite instruments can take into account the viewing geometry dictated by the satellite orbit and instrumental scan characteristics. Effects such as limb-darkening are thus accounted for explicitly, although information on the magnitude of this effect can also be extracted from the simulations, as is illustrated in the following sections.

(c) *Gaseous absorption: application of the correlated- k technique*

Gaseous absorption is parametrized using the correlated k -distribution method (Goody *et al.* 1989; Lacis and Oinas 1991; Fu and Liou 1992), extended to include the instrument spectral response (Edwards and Francis 2000). The correlated- k technique has previously been applied within the framework of the Edwards–Slingo code by Cusack *et al.* (1999) and Zhong and Haigh (2001), and has also been used in other climate and NWP model radiation schemes (e.g. Mlawer *et al.* 1997).

Following Edwards and Francis (2000) the band transmittance for a homogeneous atmosphere is written as

$$T_\phi = \frac{1}{F_\phi} \int_{\Delta\nu} t(\nu)\phi(\nu) d\nu \quad (4)$$

where $t(\nu)$ is the monochromatic transmittance and

$$F_\phi = \int_{\Delta\nu} \phi(\nu) d\nu. \quad (5)$$

A frequency distribution function, $h_\phi(k)$, is formed such that $h_\phi(k) dk$ is the fraction, $\phi(\nu) d\nu/F_\phi$, of the integration range over which the absorption coefficient lies between k and $k + dk$. The cumulative distribution function (the g -distribution) is then defined as

$$g_\phi(k) = \int_0^k h_\phi(k') dk' \quad (6)$$

with its inverse, $k(g)$, being referred to as the k -distribution. In this way, the spectral variation of the instrument response is included directly in the derivation of the k -distribution. This is different from the approximate method used by Kratz (1995) and Kratz and Rose (1999), in that they divided the channel into a small number of subintervals, over which the instrument response is assumed to be constant.

Edwards and Francis (2000) also suggest that the spectral variation of the Planck function can be accounted for by treating it in a similar manner to their method for including an instrument spectral response. This allows the Planck function and the

instrument response variation to be considered together, as a ‘combined filter’, and the band transmittance is then given by

$$T_{\phi,p} = \frac{1}{F_{\phi,p}} \int_{\Delta\nu} t(\nu)p(\nu)\phi(\nu) d\nu \quad (7)$$

where

$$F_{\phi,p} = \int_{\Delta\nu} \phi(\nu)p(\nu) d\nu \quad (8)$$

and

$$p(\nu, \Theta) = \frac{B(\nu, \Theta)}{B(\bar{\nu}, \Theta)}. \quad (9)$$

$B(\nu, \Theta)$ is the Planck function at temperature Θ and $\bar{\nu}$ is the wave number corresponding to the peak instrument response. The probability density function, g -distribution and k -distribution are then defined as for an instrument response alone. This methodology is employed to create spectral files appropriate to the satellite channels we wish to simulate.

(d) *Calculation of absorption coefficients and the g -quadrature*

The absorption coefficients are calculated at a wave-number resolution of 0.002 cm^{-1} using a Voigt lineshape (Schreier 1992) and a line cut-off of 25 cm^{-1} for all gases. All spectral line data are taken from the 1996 version of the HITRAN database (Rothman *et al.* 1998).

The basic approximation of the correlated- k technique is to extend the k -distribution approach to inhomogeneous atmospheres by assuming that the mapping from wave-number space to cumulative probability space is the same for all atmospheric layers. In practice we assume that the k -distribution for any given atmospheric conditions is correlated with that at specified reference conditions, namely the peak of the heating rate in a standard atmosphere (Chou *et al.* 1993). For a given satellite channel, the absorption coefficients for each of the gases required are calculated at the reference conditions and sorted into ascending order to produce the k -distribution, i.e. k as a function of g , with g defined as above to take into account the variation of both the instrument response and the Planck function for the channel. Note that the instrument response functions are generally only available at a limited number of discrete points and need to be interpolated to the spectral resolution of the absorption coefficients.

The relatively smooth and monotonic nature of the g -distribution (and hence also of the k -distribution) means that in practice the transmittance can be calculated using only a small number of points in the range zero to one. In this work the g -quadrature is determined by dividing the distribution into equal intervals of $\Delta \log_{10}(k)$ and calculating the mean absorption coefficient for each interval. For reasons of computational speed we choose (somewhat arbitrarily) to limit the maximum number of terms to ten, although in many cases fewer terms are sufficient to calculate the transmission to an acceptable level of accuracy. This done, the transmittance between heights z_1 and z_2 in an inhomogeneous atmosphere can then be calculated as

$$T = \sum_{j=1}^n \exp \left(- \int_{z_1}^{z_2} \bar{k}_j \rho dz \right) \Delta g_j \quad (10)$$

where ρ is the density of the absorber, n is the number of terms chosen, \bar{k}_j is the mean absorption coefficient for the j th interval and $\Delta g_j = g_j - g_{j-1}$, with $g_0 = 0$, $g_n = 1$.

Having chosen the reference conditions, (p_r, Θ_r) and selected the g -quadrature, the temperature and pressure dependence of the absorption coefficients now needs to be determined. The absorption coefficients are calculated over a range of temperatures and pressures representative of real atmospheric conditions, and for each g -interval the mean absorption coefficient is fit to a scaling function of the form

$$\bar{k}_j(p, \Theta) = \bar{k}_j(p_r, \Theta_r)(p/p_r)^{m_j} f(\Theta; \Theta_r) \quad (11)$$

where

$$f(\Theta; \Theta_r) = 1 + a_j \left(\frac{\Theta - \Theta_r}{\Theta_r} \right) + b_j \left(\frac{\Theta - \Theta_r}{\Theta_r} \right)^2. \quad (12)$$

The coefficients a_j , b_j and m_j are obtained by fitting transmittances across a wide range of absorber amounts. The mean absorption coefficients for each interval, the interval widths and the fitting parameters, along with the reference conditions, are stored in the spectral file. For the water vapour continuum, version 2.1 of the CKD formulation (Clough *et al.* 1989) is used. To be consistent with this formulation, water vapour line absorption within the cut-off is reduced by its value at 25 cm^{-1} from the line centre. The foreign-broadened continuum absorption is included in the treatment of the water vapour line absorption. The self-broadened absorption is treated separately, but in a similar manner to the line absorption. In this case only one term (i.e. one g -interval from zero to unity) is used and the scaling function is again a power law in pressure and a quadratic in temperature.

(e) Representation of cloud properties

The optical properties of cloud water droplets and ice particles are calculated from parametrizations depending on the effective radius and mass mixing ratios of water and ice. In the simulations shown here the functional form of the parametrizations used is that of Slingo (1989), although other forms are available. The actual fits are re-calculated for the particular channels chosen; the pre-processor includes the capability to re-calculate the coefficients for any desired spectral resolution. Firstly, a Mie scattering code is run for a range of physically reasonable size distributions at a large number of discrete wavelengths. The optical properties are then averaged, suitably weighted, across the spectral band. The required coefficients for the chosen parametrization are determined by fitting to these data and are then stored in the spectral file. The full details of this procedure, together with some specific examples, can be found in Edwards and Slingo (1996).

In the examples discussed here, ice crystals have been assumed to be spheres with an effective radius of $30 \mu\text{m}$, and a Henyey–Greenstein phase function has been used. Maximum overlap is used for convective or layer cloud occurring alone, while minimum overlap is used for the two types occurring together.

3. APPLICATION TO METEOSAT INFRARED CHANNELS

The methodology described in the previous section is now applied to the Meteosat 7 infrared window and water vapour channels. The window channel contains weak absorption lines of water vapour, CO_2 and ozone and has a peak weighting function near the surface, while the water vapour channel is dominated by strong water vapour absorption lines and measures radiation emanating from typically around 200–500 hPa (although in extremely dry atmospheres the emission can originate from lower layers). The utility of both of these channels for model validation studies has previously been

TABLE 1. CORRELATED- k PARAMETERS FOR THE METEOSAT 7 INFRARED (IR) WINDOW AND WATER VAPOUR CHANNELS

Channel	Spectral range (cm^{-1})	Gases included	Reference pressure (hPa)	Reference temperature (K)	g -quadrature	No. of terms
IR window	770–990	H ₂ O	1000	290	$\Delta \log(k) = 1$	5
		CO ₂	500	250	$\Delta \log(k) = 2$	3
		O ₃	60	230	$\Delta \log(k) = 4$	3
Water vapour	1350–1850	H ₂ O	500	250	$\Delta \log(k) = 0.5$	10

Note that the foreign-broadened water vapour continuum is included with the line absorption. The self-broadened continuum is treated separately and is represented by one term, with the reference conditions being the same as those for the line absorption.

demonstrated by Morcrette (1991), Schmetz and van de Berg (1994) and Roca *et al.* (1997).

The correlated- k techniques for representing gaseous absorption together with an instrument spectral response were used to produce spectral files appropriate to the infrared window and water vapour channels. The channels were each treated as a single spectral band. Off-line calculations for a range of standard atmospheres were then performed to test the accuracy of the correlated- k method against simulations at much higher spectral resolution.

Table 1 lists the most important parameters for these calculations. Figures 1 and 2 show examples of applying the correlated- k method to water vapour absorption in the two channels. The contrast between weak absorption in the window channel with the strong absorption in the water vapour channel is evident from Figs. 1(a) and 2(a). A consequence of this is that twice as many k terms (ten as opposed to five in the window channel) are required in the water vapour channel in order to calculate the radiances to the same level of accuracy. Note that in the representation of gaseous overlap normally used in the Edwards–Slingo code (Edwards 1996) full quasi-monochromatic calculations are performed for the major absorber in a band, with absorption by minor gases being computed by a number of faster subsidiary calculations. The speed of the calculation is thus determined by the number of k terms used to represent the major absorbing gas.

Table 2 compares the simulation of top-of-atmosphere, nadir, equivalent black-body brightness temperatures (brightness temperatures hereafter) using the correlated- k method with those obtained from a 10 cm^{-1} resolution version of the Edwards–Slingo code and the GENLN2 line-by-line code (Edwards 1992) for a range of standard atmospheric profiles. The 10 cm^{-1} version of the Edwards–Slingo code typically uses between 15 and 20 terms to represent water vapour line absorption in each of its 300 spectral intervals. For both sets of reference calculations the instrument response was interpolated to the spectral resolution of the calculated radiances.

These results indicate that applying the Edwards and Francis (2000) correlated- k methodology within our radiation code enables us to represent these channels as single bands with a high degree of accuracy when compared with line-by-line calculations: the maximum differences between the single band and GENLN2 brightness temperatures are 0.14 K and 0.68 K for the infrared window and water vapour channels respectively; for the other atmospheres the differences are considerably lower. It can also be noted that these differences are considerably smaller than the calibration uncertainty of the Meteosat instruments, which may be up to a few K (e.g. van de Berg *et al.* 1995). It is useful to consider these differences in relation to the information content of the measurements, in this case the difference between the surface and top-of-atmosphere

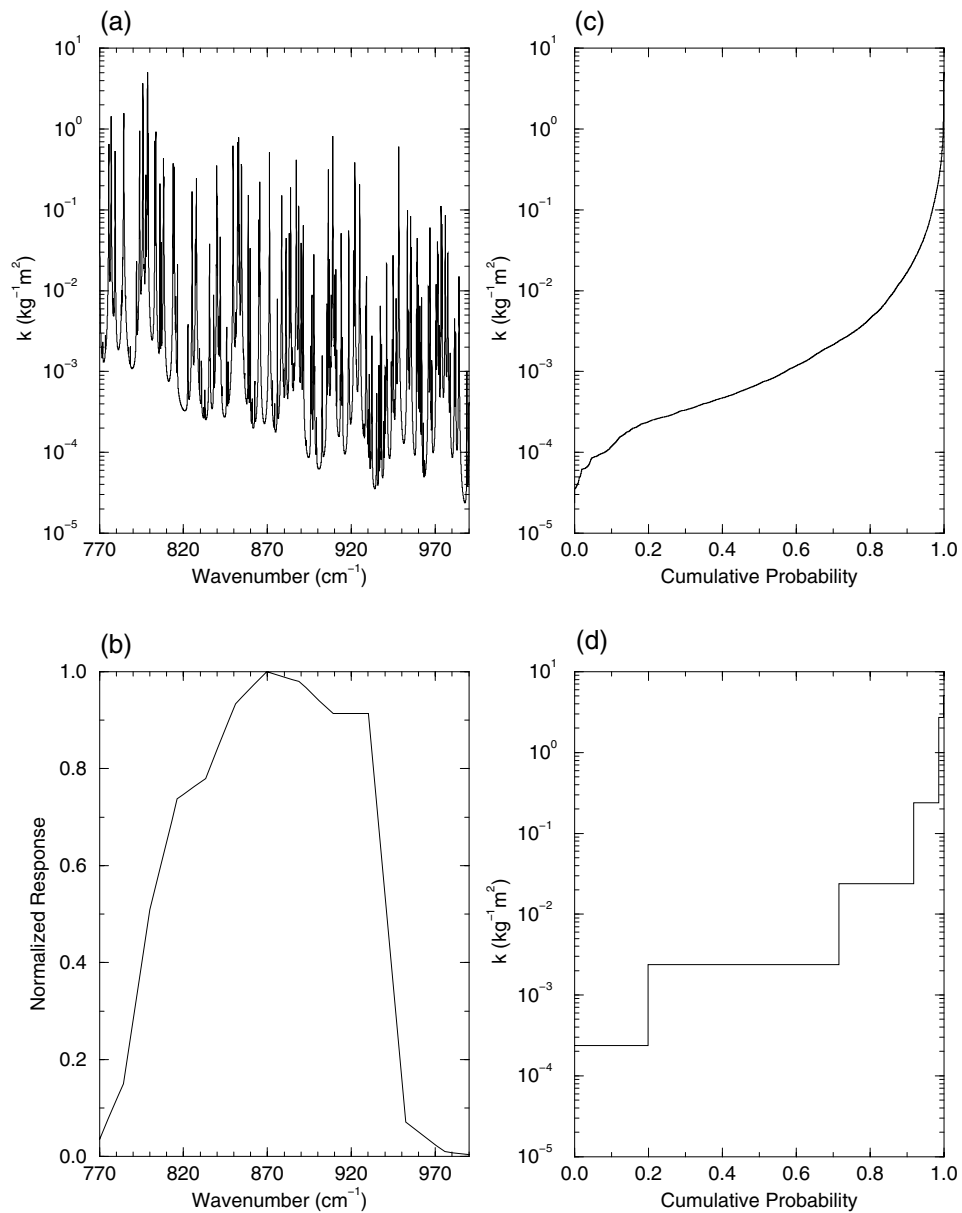


Figure 1. Application of the correlated- k method to water vapour absorption in the Meteosat 7 infrared window channel. (a) Absorption coefficient at the reference conditions of 290 K and 1000 hPa, (b) infrared window channel instrument response function, (c) exact k -distribution and (d) five-term g -quadrature. See text for further explanation.

temperatures. For the mid-latitude winter atmosphere, for example, the differences between the single band and line-by-line brightness temperatures represent 3.2% and 1.1% of the signal in the infrared window and water vapour channel respectively. The comparisons with the line-by-line calculations also confirm that the 10 cm^{-1} version of the Edwards–Slingo code is generally capable of providing a suitable reference for faster versions of the code (see also Edwards and Slingo 1996).

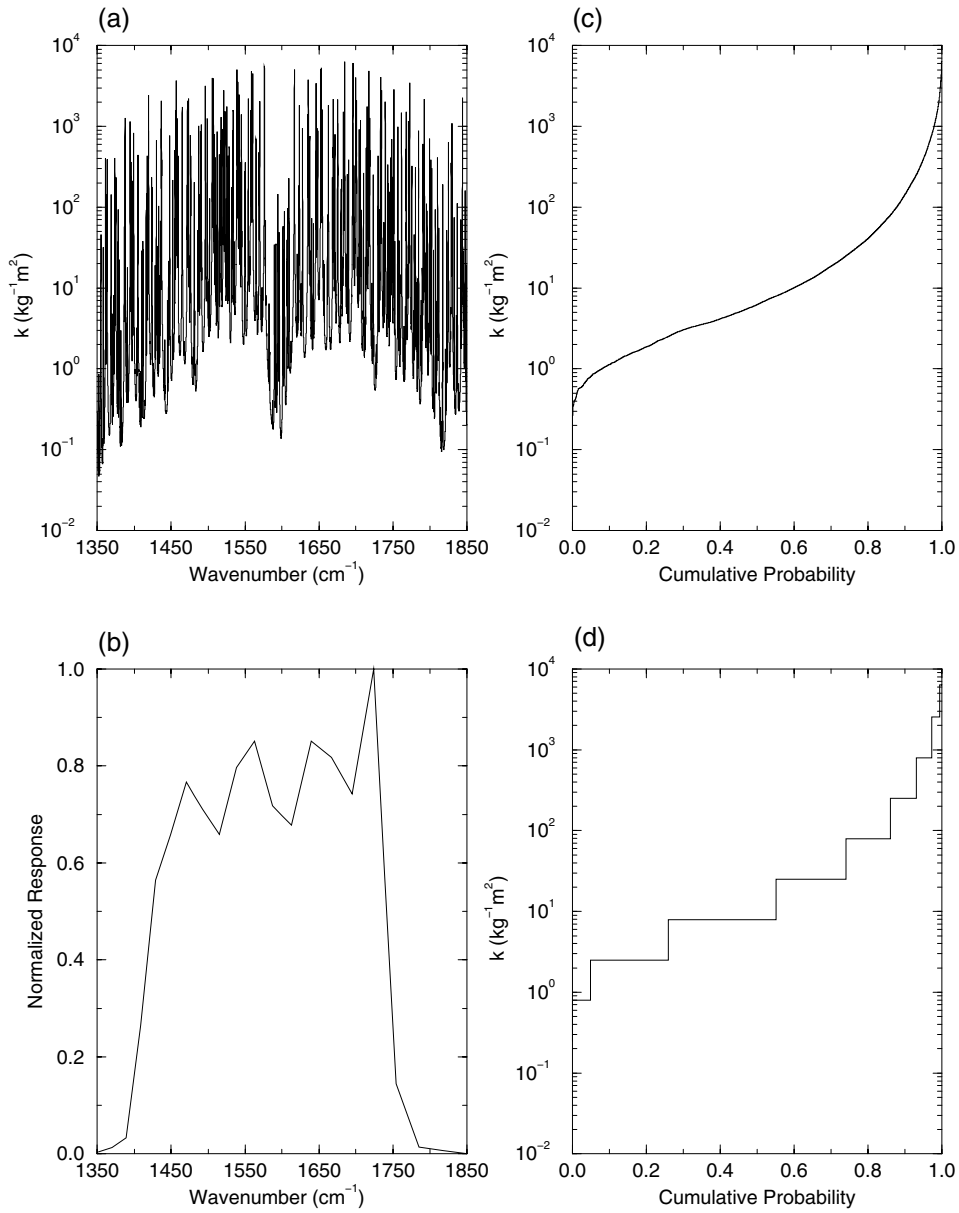


Figure 2. As Fig. 1, but for the Meteosat 7 water vapour channel. The reference conditions are 250 K and 500 hPa.

Given the dominance of water vapour as a greenhouse gas and its role in the water vapour feedback, it is important that the radiance code has the correct sensitivity to changes in water vapour concentrations. Table 3 shows the changes in top-of-atmosphere, clear-sky brightness temperatures resulting from both increasing and decreasing the water vapour amount by 25% throughout the atmospheric column. Again, comparisons are shown between the correlated- k method and the reference version of the Edwards–Slingo code. These comparisons indicate that the correlated- k method reliably

TABLE 2. SIMULATED TOP OF ATMOSPHERE, CLEAR-SKY, NADIR BRIGHTNESS TEMPERATURES (K) FOR THE METEOSAT 7 INFRARED (IR) WINDOW AND WATER VAPOUR CHANNELS FOR A RANGE OF STANDARD ATMOSPHERES. THE SINGLE-BAND CORRELATED- k METHOD IS COMPARED WITH VALUES CALCULATED USING A 10 cm^{-1} REFERENCE VERSION OF THE EDWARDS-SLINGO CODE AND THE GENLN2-4.0 LINE-BY-LINE CODE.

Atmosphere	Channel	Edwards-Slingo: correlated- k	Edwards-Slingo: reference	GENLN2
Tropical	IR window	294.83	294.85	294.85
	Water vapour	246.54	246.20	246.21
Mid-latitude summer	IR window	291.55	291.68	291.62
	Water vapour	245.22	244.84	244.87
Mid-latitude winter	IR window	271.72	271.82	271.76
	Water vapour	240.41	240.09	240.08
Sub-arctic summer	IR window	285.03	285.15	285.14
	Water vapour	242.14	242.81	242.82
Sub-arctic winter	IR window	257.04	257.10	257.18
	Water vapour	236.12	235.77	235.56

TABLE 3. CHANGES IN NADIR BRIGHTNESS TEMPERATURES (K) FOR THE METEOSAT 7 INFRARED (IR) WINDOW AND WATER VAPOUR CHANNELS RESULTING FROM INCREASES AND DECREASES (IN PARENTHESES) OF 25% TO THE WATER VAPOUR AMOUNT AT ALL ATMOSPHERIC LEVELS

Atmosphere	Channel	Edwards-Slingo: correlated- k	Edwards-Slingo: reference
Tropical	IR window	-1.46 (1.37)	-1.57 (1.47)
	Water vapour	-1.54 (2.03)	-1.55 (2.07)
Mid-latitude winter	IR window	-0.15 (0.14)	-0.16 (0.14)
	Water vapour	-1.37 (1.79)	-1.39 (1.83)

reproduces the sensitivities to humidity changes derived using the 10 cm^{-1} version of the code.

In order to simulate radiances from satellite instruments, proper account needs to be taken of the satellite viewing geometry. This is particularly important for geostationary satellites for which the viewing geometry is fixed for a given geographical location. An important consequence of observing at satellite zenith angles away from the sub-satellite point is the limb-darkening effect: as the viewing angle increases, the top-of-atmosphere radiance decreases, due to the longer pathlength through the atmosphere and the decrease of temperature with height in the troposphere. For channels in which the weighting function peaks in the stratosphere the complementary effect, known as limb-brightening, occurs. Correcting for these effects is important when merging data from different satellites to create global datasets (Hodges *et al.* 2000; Janowiak *et al.* 2001). In the present work, no correction is necessary in the simulations shown in the following section because the effect is already accounted for in the viewing geometry. However, information can easily be extracted from controlled experiments or from the differences between observed and simulated imagery that can shed light on the magnitude of the effect and its dependence on scene type. As an example, Fig. 3 shows the limb-darkening effect for the Meteosat 7 infrared window and water vapour channels. Comparisons are shown between single-band correlated- k calculations and those with the reference version of the Edwards-Slingo code for the standard tropical and mid-latitude winter atmospheres. It can be seen that the limb-darkening effect is accurately reproduced using the correlated- k version of the code: in particular, note the differences between the two channels for both atmospheric profiles and the contrast between the magnitude of the effect in the tropical and mid-latitude winter

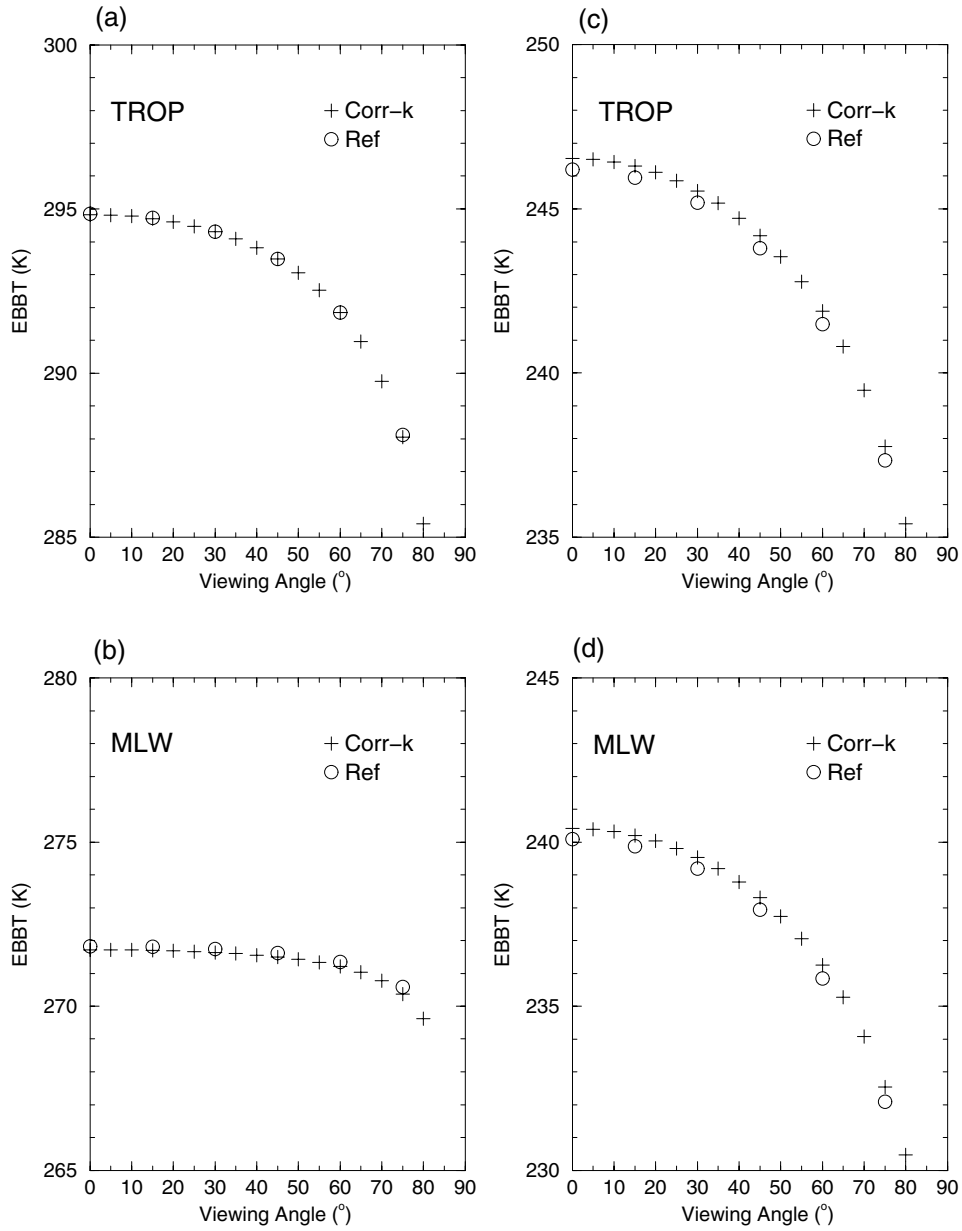


Figure 3. Clear-sky limb-darkening effect in the Meteosat 7 infrared window and water vapour channels for tropical and mid-latitude winter atmospheres. Crosses show calculations using the single band correlated- k method, circles show calculations with the reference version of the Edwards-Slingo code. (a) Infrared window channel, tropical atmosphere; (b) infrared window channel, mid-latitude winter atmosphere; (c) water vapour channel, tropical atmosphere; and (d) water vapour channel, mid-latitude winter atmosphere.

atmospheres for the infrared window channel. Similar results can be obtained for cloudy cases, although it should be remembered that, since the radiation code assumes that the atmosphere is plane parallel, three-dimensional (3-D) effects would not be included explicitly.

The results of the tests presented in this section indicate that using the Edwards and Francis (2000) correlated- k methodology to parametrize the gaseous absorption within our radiation code enables us to represent the Meteosat 7 infrared and water vapour channels as single bands in a way that produces very accurate results when compared with both line-by-line calculations and simulations using a reference (10 cm^{-1}) version of the code. Moreover, these results are found to be robust over a wide range of atmospheric conditions.

4. SIMULATIONS WITH THE UNIFIED MODEL

(a) *Forecast model*

The correlated- k methodology is now applied to simulations of Meteosat 7 infrared and water vapour channel radiances using the current global forecast version of the Unified Model (Cullen 1993), which has a horizontal resolution of approximately 0.83° (longitude) \times 0.55° (latitude) on a regular grid and 30 vertical levels. The horizontal grid is equivalent to a resolution of approximately 60 km at mid latitudes and 90 km in the tropics. The dynamics, cloud and convection schemes are described by Cullen and Davies (1991), Smith (1990), and Gregory and Rowntree (1990) respectively. Since March 1999 data assimilation has been carried out using a 3-D variational analysis scheme (Lorenz *et al.* 2000). The analysis system uses a wide variety of observation types: surface data (from land stations, ships and buoys), radiosondes, aircraft observations, satellite winds (derived from geostationary imagery and the European Remote Sensing Satellite scatterometer) and satellite sounding data (Advanced TIROS Operational Vertical Sounder).

Figure 4 shows simulations of the Meteosat 7 infrared window and water vapour channel brightness temperatures respectively for 12 GMT 4 September 2001. These simulations used the global forecast model analysis fields for this time, but since cloud fields are not present in the analysis, the simulations are based on a single time-step integration of the model from the analyses, which allows the cloud fields to be generated by the model's cloud scheme. In both cases the observed brightness temperatures, which have been averaged onto the model grid, are also shown, as are the differences between the model and the observations.

Consider the infrared window channel first (Figs. 4(a) and 4(b)). At these wavelengths ($\sim 10\text{--}13\ \mu\text{m}$) the signal emanates mainly from either the surface or the tops of (opaque) clouds. The main features seen in the observations are clearly present in the simulation: e.g. the large-scale cloud systems at mid latitudes and in the tropics, the major deserts and the sub-tropical oceanic regions where the clouds are low and warm, so that their impact on the brightness temperature is small, though clearly visible in the observations. Closer inspection does, however, reveal potentially important discrepancies. The Sahara appears to be too warm, while the desert regions over southern Africa appear to be too cool. The highest tropical clouds appear to be too warm, implying that the cloud tops are too low or that the cloud cover is underestimated. There are also significant errors in both the position and intensity of the convection that are probably related to errors in the analyses or, over Africa, to deficiencies in the simulation of the diurnal cycle of tropical convection over land (Ringer 1998; Yang and Slingo 2001). Differences in the precise locations of some of the large-scale mid-latitude cloud systems can also be seen.

Now consider the water vapour channel simulation (Figs. 4(d) and 4(e)). In clear skies, the signal at these wavelengths ($\sim 5.4\text{--}7.4\ \mu\text{m}$) is sensitive to atmospheric water

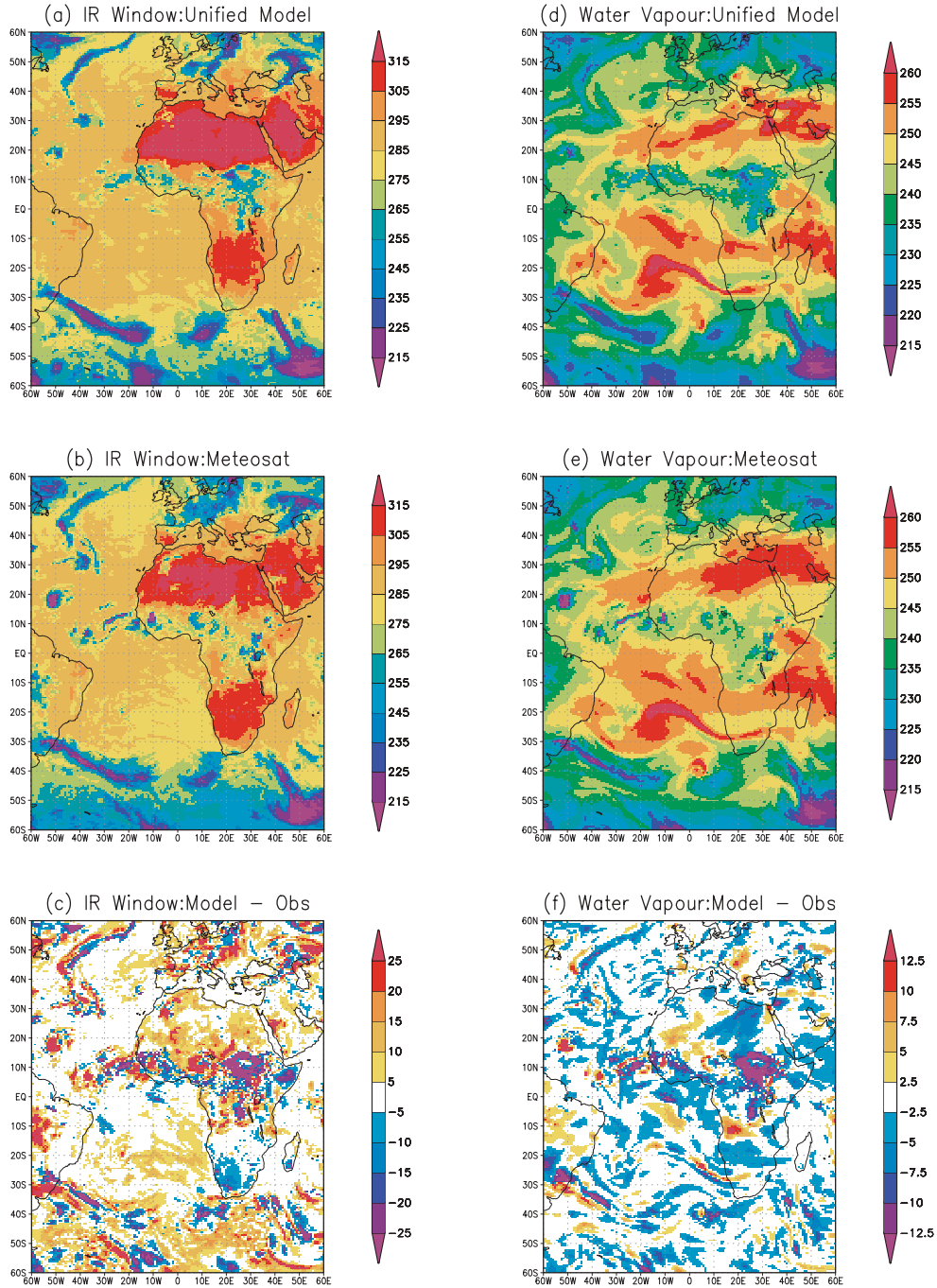


Figure 4. Unified Model simulations of the (a)–(c) Meteosat 7 infrared window and (d)–(f) water vapour channels for 12 GMT 4 September 2001. (a) and (d) Simulated brightness temperatures (K), (b) and (e) observed brightness temperatures (K), and (c) and (f) model – observation differences (K).

vapour in the mid-troposphere, the exact peak of the weighting function depending on the temperature and humidity profiles and the satellite viewing angle. Clouds below this level are obscured by the water vapour, but high-level clouds are visible and in this case the measurement is primarily influenced by the cloud-top temperature, cloud optical properties and the residual water vapour above the cloud. The general structure of the observed field is again seen to be well simulated in the model, in part due to the use of both conventional and satellite data within the analysis system and because the water vapour field is strongly influenced by the atmospheric dynamics, particularly at mid latitudes. Deficiencies in the representation of high cloud over Africa are again apparent and there are some discrepancies over the Sahara and Arabian deserts. Elsewhere, however, the features identified in the observed brightness-temperature field are reproduced by the model. Note, for example, the dry slot over the sub-tropical Atlantic and the large-scale cloud fields over the southern hemisphere mid-latitude oceans.

The difference maps (Figs. 4(c) and 4(f)) help to illustrate some of these points further. In the absence of cloud the window channel brightness temperature approaches the surface temperature, so that differences between the model and observed cloud field can lead to very large (over 30 K) differences between the simulated and observed brightness temperatures. This clearly occurs over Africa but is also apparent at mid latitudes, where slight errors in the positioning of large-scale cloud systems leads to a pattern of large positive and negative differences. Even in areas where the cloud signal is small, such differences can provide useful information: e.g. the positive differences off the west coast of southern Africa indicate the absence of low cloud in the model over this region. In the strongly absorbing water vapour channel, where the emission typically comes from around 500 hPa, differences are generally smaller, although discrepancies of more than 20 K between the observed and simulated brightness temperatures can occur where high cloud is misrepresented in the model, e.g. over Africa and the southern Atlantic. Overall, the modelled brightness temperatures tend to be lower than observed in most locations (see below). It should be noted that the cloud signals seen here are considerably larger than the calibration uncertainties associated with the Meteosat channels.

While comparisons such as these between single images and their simulated equivalents clearly provide useful 'snapshots' of model behaviour, a more thorough assessment of the model can be obtained by accumulating statistics over extended periods. As an example, Figs. 5 and 6 show histograms of observed and simulated brightness temperatures and their differences for the infrared window and water vapour channels using data accumulated over 19–23 November 2001. Over land the infrared window channel simulations (Fig. 5(a)) show that the model seems to underestimate the number of grid points with brightness temperatures less than 260 K (corresponding to middle- and high-level cloud), while overestimating the number of warmer grid points. Over the ocean (Fig. 5(b)) the behaviour is somewhat different: the highest, coldest clouds (<230 K) are overestimated, middle- and low-level clouds are underestimated (240–270 K) and the number of points with highest brightness temperature are again overestimated. The equivalent water vapour channel histograms are shown in Figs. 5(c) and 5(d). These also show the number of the coldest brightness temperatures (<220 K) to be underestimated by the model over land and overestimated over the ocean. Otherwise, over both land and ocean the warmest (clear sky) brightness temperatures are generally underestimated while the coolest are overestimated. The difference histograms for this time period (Fig. 6) show a clear contrast between the two channels. The large differences in the infrared window already noted above, which can arise because of positional errors of

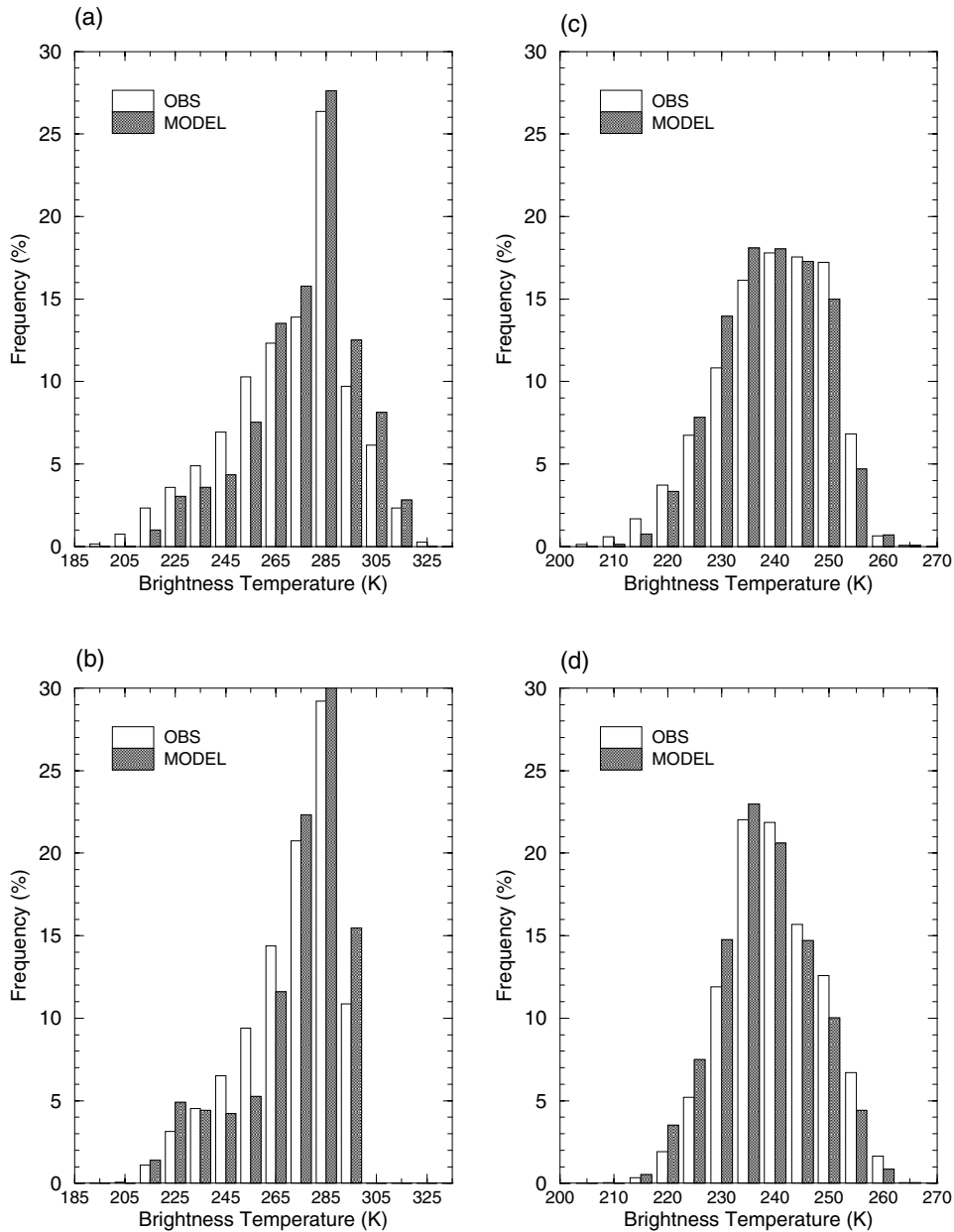


Figure 5. Histograms of observed and simulated brightness temperatures for the Meteosat 7 (a) and (b) infrared window and (c) and (d) water vapour channels for 19–23 November 2001 over (a) and (c) land and (b) and (d) ocean.

cloud systems, are illustrated by the long tails in the distributions and the large root-mean-square (r.m.s.) values over both land and ocean. Over land, of course, errors in the surface temperature, particularly over desert regions, also contribute to the errors in the brightness temperature. The distribution over the ocean is more symmetric and the mean difference, which is positive in both cases, is roughly 40% of that over land. Positional errors lead to smaller differences in the water vapour channel and this is

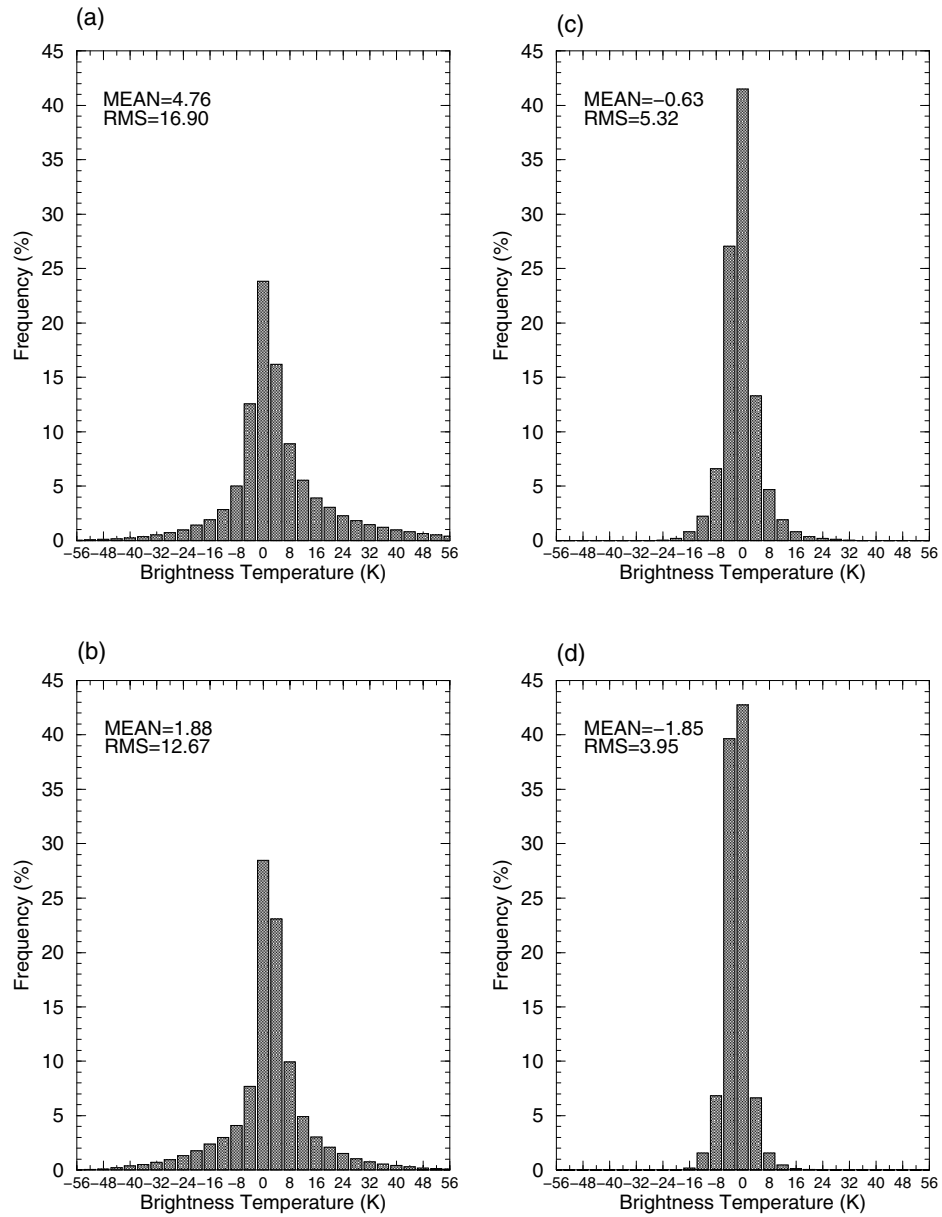


Figure 6. Histograms of differences between simulated and observed brightness temperatures for the Meteosat 7 (a) and (b) infrared window and (c) and (d) water vapour channels for 19–23 November 2001 over (a) and (c) land and (b) and (d) ocean.

reflected in the resulting histograms (Figs. 6(c) and 6(d)) and smaller r.m.s. values. The mean differences suggest that the model is too moist, particularly over the ocean, consistent with generally negative differences seen in Fig. 4(f). These results illustrate the high information content of comparisons between simulated and observed brightness temperatures, in both spectral regions. There is considerable potential for evaluating the model's simulation of clouds, water vapour and the land surface and this will be exploited in future studies.

(b) *Sensitivity studies*

Given the numerical cost of performing the radiance simulations, it is important to explore whether economies can be made that do not seriously compromise results. Two sensitivity experiments are described here.

Firstly, we consider the effect of scattering in the Meteosat infrared window and water vapour channels. Absorption due to water vapour and water and ice particles dominates in the long wave and it is a common assumption to neglect scattering, particularly in the fast-forward models used in data assimilation but also in NWP and climate models. However, the effect of scattering in the long wave has been shown to be non-negligible in the calculation of fluxes (e.g. Chou *et al.* 1999) and the spectral variation of scattering can be exploited for remote sensing of cloud properties (e.g. Strabala *et al.* 1994). On the other hand, the neglect of scattering leads to significant gains in computing time, as multiple-scattering calculations are very expensive.

Figures 7(a) and 7(b) show the effect of neglecting scattering in the two Meteosat 7 channels for the simulations shown in Fig. 4. Scattering reduces the cloud-top emission due to upward radiation being backscattered deeper into the cloud, hence the positive differences seen in both cases. In the infrared window channel differences exceed 5 K, indicating the potential importance of scattering at these wavelengths. It may be that a more accurate description of the single-scattering properties of ice crystals would lead to smaller differences than those seen here, and this will be explored. The effect of scattering needs to be considered in terms of the information content of the measurement: for a cloud at 240 K above a surface at 300 K, for example, a scattering effect of 3 K represents 5% of the brightness-temperature depression due to the cloud. The decision to include or neglect scattering clearly depends on the particular application. Given that such large differences between modelled and observed brightness temperatures can occur due to positional errors of cloud systems (Fig. 4(c)), assessing the significance of the scattering effect in this context is not straightforward and would require a statistical approach similar to that shown in Figs. 5 and 6. In the strongly absorbing water vapour channel scattering is much less important and can probably be neglected in most circumstances.

We next consider the effect of varying the order of truncation, L (see Eqs. (2) and (3)) on the simulation of the infrared window and water vapour brightness temperatures. This parameter represents the specification of the angular variation of radiance field: as L is increased more terms are used to describe the angular variation, increasing the computational cost of the calculation, which is proportional to L^3 . Figures 7(c) and 7(d) show the effect of varying L from 3 to 9, thus increasing the computational burden by a factor of 27. Scattering is included in both cases. In these long-wave channels the radiance field varies fairly smoothly with angle and a low order of truncation is likely to be sufficient in many applications; this is especially true for the water vapour channel. In the short wave, of course, this is clearly not the case and great care will be needed when deciding how to specify the anisotropy of the radiance field.

5. DISCUSSION

A facility to simulate satellite channel radiances within the Met Office Unified Model has been developed, allowing us to adopt a truly model-to-satellite approach to validation studies and providing us with a valuable tool for assessing the representation of physical processes within the model. The radiance code has been developed within the framework of the Edwards and Slingo (1996) two-stream code and retains a similar level of generality and flexibility. Radiances are calculated using a spherical harmonics

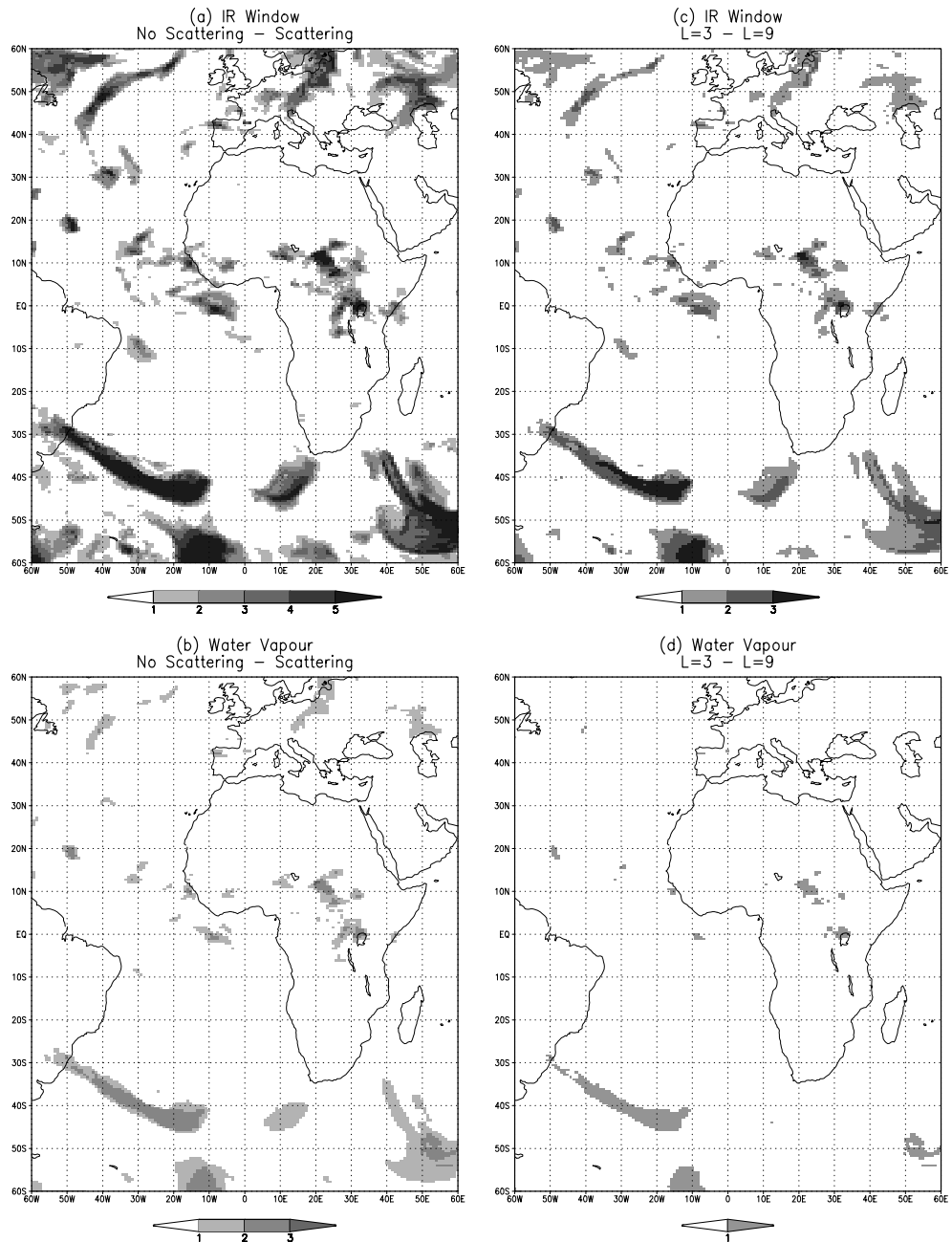


Figure 7. (a) and (b) Effect of neglecting scattering (K) for (a) infrared window and (b) water vapour channel simulations shown in Fig. 4. (c) and (d) Effect of reducing truncation (K) from $L=9$ to $L=3$ (see text) for (c) infrared window and (d) water vapour channel simulations shown in Fig. 4.

method. An extension of the correlated- k methodology proposed by Edwards and Francis (2000), which includes the spectral variation of an instrument response function, is used to represent gaseous absorption. Satellite viewing geometry is taken into account in the radiance calculation, so that effects related to it, such as limb-darkening, are included explicitly. The code allows radiances to be calculated for both the short-wave and long-wave parts of the spectrum, although the work presented here deals only with the simulation of long-wave channels.

Off-line simulations for a range of standard atmospheres and viewing geometries indicate that the treatment of satellite channels as a single spectral band enables radiances to be calculated to a high degree of accuracy compared to high spectral resolution calculations. For reasons of computational speed, a single band is generally used when simulating satellite channel radiances within the Unified Model, although it is possible to divide a channel into several bands if the single band representation is judged not to be sufficiently accurate. The bands can be of arbitrary spectral width, so that in principle the methodology could be applied to the simulation of high-resolution instruments such as the AIRS* (Aumann and Pagano 1996) and IASI† (Cayla 1993). This would, of course, be subject to the limitations of the correlated- k technique, in particular the assumption of correlation of the absorption coefficients between vertical layers. For spectral bands where this approximation starts to break down (i.e. the accuracy obtained is inadequate for the particular application) improvements to the vertical correlation can be achieved using the method of Oinas (1993), an application of which was described by Edwards and Francis (2000). Alternatively, mapping transformation approaches (West *et al.* 1990), which do not rely on the assumption of vertical correlation, could be employed.

The methodology has been illustrated with simulations of the Meteosat 7 water vapour and infrared channels using the current version of the Met Office global forecast model. These examples demonstrate the utility of this approach for using satellite data for model validation studies: according to the channels chosen, particular physical processes (e.g. clouds, upper tropospheric moisture, and surface phenomena) can be isolated. Finally, it should be noted that radiance simulations augment, rather than remove the need for, comparisons with high-level products and, where possible, both approaches to model validation should be used in parallel.

ACKNOWLEDGEMENTS

This work was supported by the Department of Environment, Food and Rural Affairs under contract PECD 7/12/37. We thank Peter Rayer for providing the line-by-line calculations used in section 3, and Anthony Baran for useful discussions on scattering.

REFERENCES

- | | | |
|---|------|--|
| Aumann, H. H. and Pagano, R. J. | 1994 | Atmospheric infrared sounder on Earth Observing System. <i>Opt. Eng.</i> , 7 , 66–88 |
| Bates, J. J., Wu, X. and Jackson, D. L. | 1996 | Interannual variability of upper-tropospheric water vapour band brightness temperature. <i>J. Climate</i> , 9 , 427–438 |
| Benassi, M., Garcia, R. D. M., Karp, A. H. and Siewert, C. E. | 1984 | A high-order spherical harmonics solution to the standard problem in radiative transfer. <i>Astrophys. J.</i> , 280 , 853–864 |

* Atmospheric Infrared Sounder.

† Infrared Atmospheric Sounding Instrument.

- Cayla, F. 1993 'IASI infrared interferometer for operations and research'. In *High spectral resolution infrared remote sensing for Earth's weather and climate studies*. NATO ASI Series, Vol. I 9. Eds. A. Chedin, M. Chahine and N. Scott. Springer
- Chevallier, F. and Kelly, G. 2002 Model clouds over oceans as seen from space: comparison with geostationary imagery in the 11 μm window channel. *Mon. Weather Rev.*, **130**, 712–722
- Chou, M.-D., Ridgway, W. L. and Yan, M.-H. 1993 One-parameter scaling and exponential sum fitting for water vapor and CO₂ infrared transmission functions. *J. Atmos. Sci.*, **50**, 2294–2303
- Chou, M.-D., Lee, K.-T., Tsay, S.-C. and Fu, Q. 1999 Parametrization for cloud longwave scattering for use in atmospheric models. *J. Climate*, **12**, 159–169
- Clough, S. A., Kneizys, F. X. and Davies, R. W. 1989 Line shape and the water vapour continuum. *Atmos. Res.*, **23**, 229–241
- Cullen, M. J. 1993 The unified forecast/climate model. *Meteorol. Mag.*, **122**, 81–94
- Cullen, M. J. and Davies, T. 1991 A conservative split-explicit integration scheme with fourth-order horizontal advection. *Q. J. R. Meteorol. Soc.*, **117**, 993–1002
- Cusack, S., Edwards, J. M. and Crowther, J. M. 1999 Investigating *k*-distribution methods for parameterizing gaseous absorption in the Hadley Centre Climate Model. *J. Geophys. Res.*, **104**, 2051–2057
- Duvel, J.-Ph., Morcrette, J.-J. and Klinker, E. 1996 'Evaluation of the spatio-temporal variability of tropical convection in GCMs by using geostationary satellite data'. In *Climate sensitivity to radiative perturbations: physical mechanisms and their validation*. NATO ASI Series, Vol. I 34. Ed. H. Le Treut. Springer
- Edwards, D. P. 1992 'A general line-by-line atmospheric transmittance and radiance model'. NCAR Technical Note NCAR/TN-367+STR
- Edwards, D. P. and Francis, G. L. 2000 Improvements to the correlated-*k* radiative transfer method: Application to satellite infrared sounding. *J. Geophys. Res.*, **105**, 18135–18156
- Edwards, J. M. 1996 Efficient calculation of infrared fluxes and cooling rates using the two-stream equations. *J. Atmos. Sci.*, **53**, 1921–1932
- Edwards, J. M. and Slingo, A. 1996 Studies with a flexible new radiation code. I: Choosing a configuration for a large-scale model. *Q. J. R. Meteorol. Soc.*, **122**, 689–719
- Engelen, R. J., Fowler, L. D., Gleckler, P. J. and Wehner, M. F. 2000 Sampling strategies for the comparison of climate model calculated and satellite observed brightness temperatures. *J. Geophys. Res.*, **105**, 9393–9406
- English, S. J., Renshaw, R. J., Dibben, P. C., Smith, A. J., Rayer, P. J., Poulsen, C., Saunders, F. W. and Eyre, J. R. 2000 A comparison of the impact of TOVS and ATOVS satellite sounding data on the accuracy of numerical weather forecasts. *Q. J. R. Meteorol. Soc.*, **126**, 2911–2931
- Eyre, J. R. 1991 'A fast radiative transfer model for satellite sounding systems'. ECMWF Tech. Memo. No. 176. ECMWF Reading, UK
- Fu, Q. and Liou, K. N. 1992 On the correlated *k*-distribution method for radiative transfer in nonhomogeneous atmospheres. *J. Atmos. Sci.*, **49**, 2139–2156
- Geer, A. J., Harries, J. E. and Brindley, H. E. 1999 Spatial patterns of climatic variability in upper-tropospheric water vapor radiances from satellite data and climate model simulations. *J. Climate*, **12**, 1940–1955
- Goody, R., West, R., Chen, L. and Crisp, D. 1989 The correlated-*k* method for radiation calculations in nonhomogeneous atmospheres. *J. Quant. Spectrosc. Radiat. Transfer*, **42**, 539–550
- Goody, R., Anderson, J. and North, G. 1998 Testing climate models: An approach. *Bull. Am. Meteorol. Soc.*, **79**, 2541–2549
- Gregory, D. and Rowntree, P. R. 1990 A mass flux convection scheme with representation of cloud ensemble characteristics and stability-dependent closure. *Mon. Weather Rev.*, **118**, 1483–1506
- Hodges, K. I., Chappell, D. W., Robinson, G. J. and Yang, G. 2000 An improved algorithm for generating global window brightness temperatures from multiple satellite infrared imagery. *J. Atmos. Ocean Technol.*, **17**, 1296–1312
- Janowiak, J. E., Joyce, R. J. and Yarosh, Y. 2001 A real-time global half-hourly pixel-resolution infrared dataset and its applications. *Bull. Am. Meteorol. Soc.*, **82**, 205–217
- Kratz, D. P. 1995 The correlated *k*-distribution technique as applied to the AVHRR channel. *J. Quant. Spectrosc. Radiat. Transfer*, **53**, 501–517

- Kratz, D. P. and Rose, F. 1999 Accounting for molecular absorption within the spectral range of the CERES window channel. *J. Quant. Spectrosc. Radiat. Transfer*, **61**, 83–95
- Lacis, A. A. and Oinas, V. 1991 A description of the correlated- k distribution method for modeling nongray gaseous absorption, thermal emission, and multiple scattering in vertically inhomogeneous atmospheres. *J. Geophys. Res.*, **96**, 9027–9063
- Lorenc, A. C., Ballard, S. P., Bell, R. S., Ingleby, N. B., Andrews, P. L. F., Barker, D. M., Bray, J. R., Clayton, A. M., Dalby, T., Li, D., Payne, T. J. and Saunders, F. W. 2000 The Met. Office global 3-dimensional variational data assimilation scheme. *Q. J. R. Meteorol. Soc.*, **126**, 2991–3012
- Mlawer, E. J., Taubman, J., Brown, P. D., Iacono, M. J. and Clough, S. A. 1997 Radiative transfer for inhomogeneous atmospheres: RRTM, a validated correlated- k model for the longwave. *J. Geophys. Res.*, **102**, 16663–16682
- Morcrette, J.-J. 1991 Evaluation of model-generated cloudiness: Satellite observed and model-generated diurnal variability of brightness temperature. *Mon. Weather Rev.*, **119**, 1205–1224
- Nakajima, T. and Tanaka, M. 1988 Algorithms for radiative intensity calculations in moderately thick atmospheres using a truncation approximation. *J. Quant. Spectrosc. Radiat. Transfer*, **40**, 51–60
- Oinas, V. 1993 ‘Improved correlation in correlated k ’. In *IRS '92: Current problems in atmospheric radiation*. Eds. S. Keevalik and O. Karner. A. Deepak
- Pope, V. D., Gallani, M. L., Rowntree, P. R. and Stratton, R. A. 2000 The impact of new physical parametrizations in the Hadley Centre climate model: HadAM3. *Clim. Dyn.*, **16**, 123–146
- Ringer, M. A. 1998 ‘Tropical convective rainfall in the Global UM: Initial comparisons with estimates derived from Meteosat IR data’. Forecasting Research Technical Report, No. 239 (Available from the Met Office, Bracknell UK)
- Roca, R., Picon, L., Desbois, M. and Le Treut, H. 1997 Direct comparison of Meteosat water vapor channel and general circulation model results. *Geophys. Res. Lett.*, **24**, 147–150
- Rothman, L. S., Rinsland, C. P., Goldman, A., Massie, S. T., Edwards, D. P., Flaud, J. M., Perrin, A., Camy-Peyret, C., Dana, V., Mandin, J. Y., Schroeder J., McCann, A., Gamache, R. R., Wattson, R. B., Yoshino, K., Chance, K. V., Jucks, K. W., Brown, L. R., Nemtchinov, V. and Varanasi, P. 1998 The HITRAN molecular spectroscopic database and HAWKS (HITRAN atmospheric workstation): 1996 edition. *J. Quant. Spectrosc. Radiat. Transfer*, **60**, 665–710
- Salathé, E. P. and Chesters, D. 1995 Variability of moisture in the upper troposphere as inferred from TOVS satellite observations and the ECMWF model analyses in 1989. *J. Climate*, **8**, 120–132
- Salathé, E. P., Chesters, D. and Sud, Y. C. 1995 Evaluation of the upper-tropospheric moisture climatology in a general circulation model using TOVS radiance observations. *J. Climate*, **8**, 2404–2414
- Schmetz, J. and van de Berg, L. 1994 Upper tropospheric humidity observations from Meteosat compared with short-term forecast fields. *Geophys. Res. Lett.*, **21**, 573–576
- Schreier, F. 1992 The Voigt and complex error function: A comparison of computational methods. *J. Quant. Spectrosc. Radiat. Transfer*, **48**, 743–762
- Slingo, A. 1989 A GCM parameterization for the shortwave radiative properties of water clouds. *J. Atmos. Sci.*, **46**, 1419–1427
- Smith, R. N. B. 1990 A scheme for predicting layer clouds and their water contents in a GCM. *Q. J. R. Meteorol. Soc.*, **116**, 435–460
- Soden, B. J. and Bretherton, F. P. 1994 Evaluation of the water vapor distribution simulated in GCMs using satellite observations. *J. Geophys. Res.*, **99**, 1187–1210
- Soden, B. J. and Fu, R. 1995 A satellite analysis of deep convection, upper-tropospheric humidity, and the greenhouse effect. *J. Climate*, **8**, 2333–2351

- Strabala, K. A., Ackerman, S. A. and Menzel, W. P. 1994 Cloud properties inferred from 8–12 μm data. *J. Appl. Meteorol.*, **33**, 212–229
- van de Berg, L. C. J., Schmetz, J. and Whitlock, J. 1995 On the calibration of the Meteosat water vapour. *J. Geophys. Res.*, **100**, 21069–21076
- West, R., Crisp, D. and Chen, L. 1990 Mapping transformations for broadband atmospheric radiation calculations. *J. Quant. Spectrosc. Radiat. Transfer*, **43**, 191–199
- Yang, G. Y. and Slingo J. 2001 The diurnal cycle in the tropics. *Mon. Weather Rev.*, **129**, 784–801
- Yu, W., Garand, L. and Dastoor, A. P. 1997 Evaluation of model clouds and radiation at 100 km scale using GOES data. *Tellus*, **49A**, 246–262
- Zhong, W. and Haigh, J. D. 2001 An efficient and accurate correlated- k parameterization of infrared radiative transfer for troposphere–stratosphere–mesosphere GCMs. *Atmos. Sci. Lett.*, doi:10.1006/asle.2000.0022